GEOPHYSICS, VOL. 72, NO. 4 (JULY-AUGUST 2007); P. F177–F187, 14 FIGS., 1 TABLE.
10.1190/1.2734365

Time-lapse ERT monitoring of an injection/withdrawal experiment in a shallow unconfined aquifer

Greg A. Oldenborger[1], Michael D. Knoll[2], Partha S. Routh[2], and Douglas J. LaBrecque[3]

ABSTRACT

To quantify performance of 3D time-lapse electrical resistivity tomography (ERT), a sequential injection/withdrawal experiment was designed for monitoring the pump-and-capture remediation of a conductive solute in an unconfined alluvial aquifer. Prior information is incorporated into the inversion procedure via regularization with respect to a reference model according to three protocols: (1) independent regularization involving a single reference model, (2) background regularization involving a reference model obtained via inversion of preinjection data, and (3) time-lapse regularization involving an evolving reference model obtained via inversion of data from previous experimental stages. Emplacement and sequential withdrawal of the solute is clearly imaged for all protocols. Time-lapse regularization results in greater amounts of model structure, while providing significant computational savings. ERT-estimated electrical conductivity is used to predict solute concentration and solute mass in the aquifer. At any experimental stage, we are able to estimate total solute mass in the aquifer with a maximum accuracy of 60%–85% depending on regularization protocol and survey geometry. We also estimate the withdrawn solute mass for every experimental stage (the change in mass between experimental stages). Withdrawn mass estimates are more reliable than total mass estimates and do not exhibit systematic underprediction or dependence on regularization protocol. Withdrawn mass estimates are accurate for changes in mass below 2–4 kg of potassium bromide (KBr) for horizontal and vertical dipole-dipole surveys, respectively. Estimating the withdrawn solute mass does not require background subtraction and, thus, does not require background data.

INTRODUCTION

Geophysical experiments have the ability to provide minimally invasive, nearly continuous, and spatially extensive estimates of material properties for near-surface investigations (e.g., Hyndman and Gorelick, 1996; Bentley and Gharibi, 2004; Ramirez et al., 2005). In particular, electrical resistivity tomography (ERT) can be used to image and estimate the electrical properties of the earth's subsurface. This geophysical information is used often to detect the presence or movement of water and contaminants. Although usefulness of ERT has been demonstrated in a groundwater context (Binley et al., 2002; Kemna et al., 2002; Slater et al., 2002; Singha and Gorelick, 2005), significant challenges remain in assessing how ERT can be used to routinely provide detailed and quantitative hydrogeologic information, such as solute concentration, solute mass, or changes in those quantities over time.

In a time-lapse context, we are interested in measuring the changes in geophysical properties at particular locations at different times. A major benefit of time-lapse or differential experiments is the potentially enhanced discrimination that results from interpretation of geophysical data or models with respect to some known background state. Typically, differential models are achieved via independent inversion and postinversion model differencing (e.g., Slater and Sandberg, 2000). However, it may be beneficial to incorporate information about past model states into the inversion procedure. Proposed methods of time-lapse inversion include inverting on data differences or ratios (LaBrecque and Yang, 2001; Daily et al., 2004), space-time parameterization (Day-Lewis et al., 2002), or cross-model regularization (Loke, 1999). Alternatively, without altering the data form or explicitly regularizing in time, we can effect a dependence on a previous model through regularization with respect to a reference model. However, there is limited research on the effects of in-

Manuscript received by the Editor October 18, 2006; revised manuscript received February 14, 2007; published online May 24, 2007.
[1]University of British Columbia, Department of Earth and Ocean Sciences, Vancouver, British Columbia. E-mail: goldenborger@eos.ubc.ca.
[2]Boise State University, Department of Geosciences, Boise, Idaho. E-mail: mknoll@cgiss.boisestate.edu; routh@cgiss.boisestate.edu.
[3]Multi-Phase Technologies, LLC, Sparks, Nevada. E-mail: dlabrec887@yahoo.com.

corporating knowledge about past material property distributions.

To examine the capabilities and limitations of time-lapse ERT imaging in the context of an environmental or engineering geophysical application, a potassium bromide (KBr) injection/withdrawal test was designed and conducted at the Boise Hydrogeophysical Research Site (BHRS) as a proxy for ERT detection and monitoring of pump-and-capture remediation of a conductive contaminant in an unconfined alluvial aquifer. Preinjection (background) ERT images enhance understanding of the subsurface hydrogeology in terms of porosity and preferential flow paths. For postinjection ERT data, we define three inversion protocols based on reference model regularization: (1) independent regularization involving a single reference model, (2) background regularization involving a reference model obtained via inversion of preinjection data, and (3) time-lapse regularization involving changing reference models obtained via inversion of data from previous experimental stages. The time-lapse protocol is similar to cross-model regularization (Loke, 1999) and iterative Tikhonov regularization (Hanke and Groetsch, 1998).

The different inversion protocols are compared based on the regularization trade-off parameter, the model size, and the conductivity distribution. Through simple petrophysical transforms, the ERT-estimated electrical conductivity allows for 3D time-lapse monitoring of fluid conductivity, solute concentration, total solute mass remaining in the aquifer, and withdrawn mass. The ERT results are evaluated by comparing predicted solute mass to the solute mass determined from fluid conductivity measurements of injection, discharge, and multilevel water samples.

EXPERIMENTAL DESIGN

The BHRS is a mesoscale research site developed in a common type of unconfined alluvial aquifer that is heavily utilized, but easily contaminated by anthropogenic activity. The BHRS consists of 18 multiuse boreholes emplaced in coarse sand and gravel deposits along the Boise River, Boise, Idaho (Barrash and Clemo, 2002). Figure 1 shows a schematic illustration of the central boreholes relevant to this experiment.

On the morning of day 1, a solution of 31.5 kg of KBr in approximately 3740 L of aquifer water (8420 ppm) was injected into the central borehole A1. The injection was isolated over the interval of 6.9–9.3-m depth below land surface using an inflatable packer system. The particular injection interval was chosen based on the interpretation of neutron porosity logs and core samples (Barrash and Clemo, 2002; Barrash and Reboulet, 2004) that indicate the existence of a low-porosity hydrostratigraphic unit from approximately 6.5–9.5-m depth (Figure 2). The low-porosity unit was chosen to limit down-gradient migration of the solute over the duration of the experiment. Pumping rates and volumes were designed to achieve a nominal plume size equivalent to a cylinder of approximately 2.5 m in height and 3 m in diameter. The solute tracer was sequentially withdrawn by pumping from borehole A1 in six daily stages (days 2–7), each designed to reduce the nominal plume radius by approximately 0.5-m increments. Before, during, and after the injection and withdrawal of the KBr solution, the state of the aquifer was monitored using 3D ERT and 1D water samples.

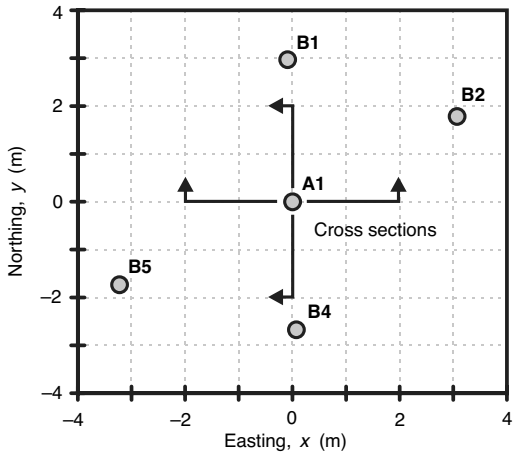

Figure 1. Schematic representation of borehole infrastructure. The lines of cross section indicate views to be illustrated in subsequent figures.

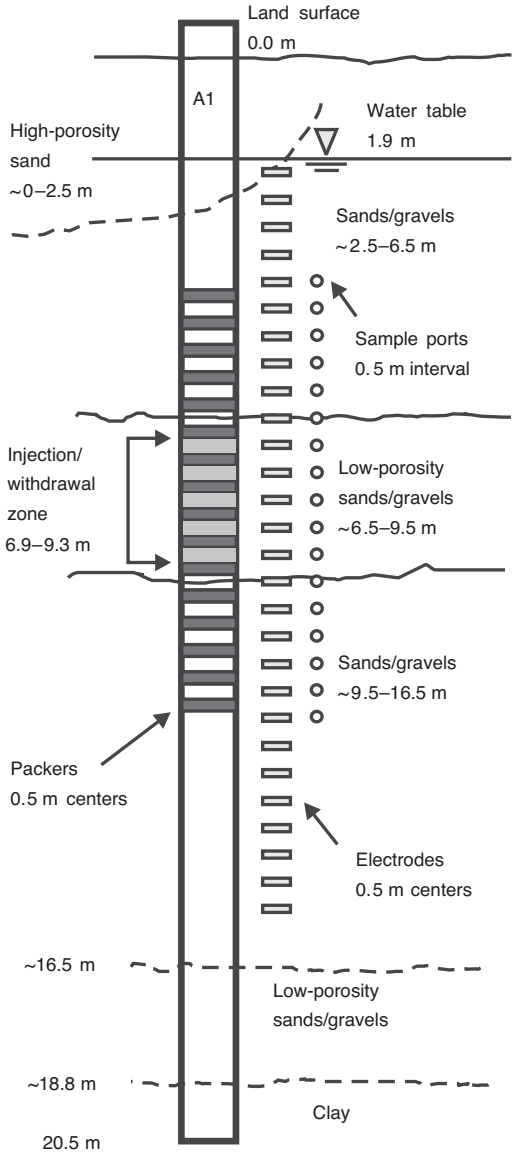

Figure 2. Schematic representation of the packer/electrode system. Air-inflated packers isolate zones of the aquifer at 0.50-m spacing. The 1D sedimentary section is based on neutron porosity logs and core samples from borehole A1 (Barrash and Reboulet, 2004).

DATA ACQUISITION AND ANALYSIS

Water sample acquisition and analysis

During each injection and withdrawal event, 30-mL water samples were acquired at variable time intervals from the pump lines at the surface. These samples were taken in conjunction with temperature, flow rate, and volume measurements to calculate injected and withdrawn mass. In addition to pump-line samples, 30-mL samples of aquifer water were collected from the multilevel system in A1 (Figure 2), and from high (7.6-m depth) and low (11.6-m depth) positions in boreholes B1, B2, B4, and B5 (Figure 1). Electrical conductivity of water samples was measured off-site using a Denver Instrument Model 250 conductivity meter, and a calibrated YSI 2-electrode conductivity probe (#3403).

Water samples were collected in the B boreholes as indicators of solute presence. None of the B-borehole water samples show fluctuations of fluid conductivity above background variability over the duration of the injection/withdrawal experiment, indicating containment of the tracer. Multilevel water samples in borehole A1 were collected to provide a 1D constraint on fluid conductivity within the aquifer. However, problems with peristaltic pump rates resulted in variable and insufficient purging of the A1 sample lines between sampling events. As such, the A1 water samples cannot be time-stamped accurately, but can be used in a qualitative fashion. Figure 3 illustrates the fluid conductivity profiles for days 0–3. Increased conductivities indicate the presence of solute along the entire sampled length of the borehole, despite injection being confined to the packed-off zone. This behavior is possibly a result of short-circuiting of the packer system by vertical fluid flow around weak packer seals and/or adjacent to the borehole in zones of incomplete natural-collapse created during emplacement of the boreholes.

Given the instantaneous nature of the injection and discharge water samples, fluid conductivity measurements for these samples are not subject to purge-time errors and can be used quantitatively to calculate solute mass in the aquifer. Electrical conductivity of the fluid is converted to KBr concentration C (mg/L) using the calibration equation

$$C = X(\sigma_f - \sigma_f^0), \qquad (1)$$

where X (mg/L)(m/mS) is an experimental calibration constant, σ_f (mS/m) is the fluid conductivity, and σ_f^0 (mS/m) is the background fluid conductivity (Hausrath et al., 2002). Measured fluid conductivities were corrected for water temperature to allow for conversion to true concentration. At the BHRS, the background aquifer water is homogeneous over the study area with an electrical conductivity of $\sigma_f^0 = 20 \pm 1$ mS/m at a temperature of 17°C, for which $X_{17} = 11.1 \pm 0.2$(mg/L)(m/mS). The temperature of the injected solution was 22°C, for which $X_{22} = 9.9 \pm 0.2$ (mg/L)(m/mS). For withdrawal stages, the temperature of the aquifer water had returned approximately to background. Pumped volumes, fluid conductivity, and solute mass are presented in Table 1. The injected mass as determined from fluid conductivity measurements is in agreement with the mass used to prepare the solution.

ERT data acquisition

Borehole A1 and the surrounding boreholes B1, B2, B4, and B5 were each instrumented with 28 electrodes spaced at 0.5-m intervals from 2.1–15.6-m depth below land surface (Figure 2). ERT data were acquired prior to injection, postinjection, and postwithdrawal for each stage of the experiment. Two distinct ERT survey geometries are considered and illustrated in Figure 4: (1) circulating skip-3 vertical dipole-dipole (e.g., Slater et al., 2002) and (2) horizontal dipole-dipole (e.g., Zhou and Greenhalgh, 2000). For the vertical di-

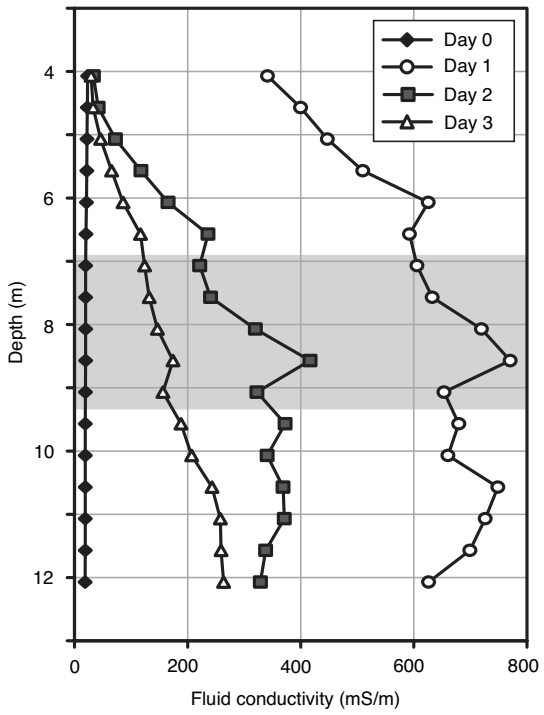

Figure 3. Fluid conductivity profiles at A1 for preinjection (day 0), postinjection (day 1), and postwithdrawal (days 2 and 3) experimental stages. The gray zone indicates the packed-off injection/withdrawal zone.

Table 1. Injection and withdrawal dates and days, injected/withdrawn volume V, fluid conductivity σ_f, solute concentration C, change in solute mass (i.e., injected or withdrawn mass) ΔM, and total solute mass remaining M. Values and errors for σ_f are reported as the mean and one standard deviation of the N samples taken during each injection or withdrawal event. Dates are for August 2004.

Date/day	V (L)	σ_f (mS/m)	N	C KBr (mg/L)	ΔM (kg)	M (kg)
9/0	0	20 ± 1	54	0	0	0
10/1	3736	873 ± 44	18	8443 ± 454	31.5 ± 1.7	31.5 ± 1.7
11/2	− 1079	488 ± 15	5	5200 ± 182	− 5.61 ± 0.20	25.9 ± 1.7
12/3	− 935	331 ± 12	3	3454 ± 146	− 3.23 ± 0.14	22.7 ± 1.7
13/4	− 767	234 ± 9	4	2375 ± 107	− 1.73 ± 0.08	21.0 ± 1.7
14/5	− 519	174 ± 9	3	1712 ± 104	− 0.89 ± 0.05	20.1 ± 1.7
15/6 AM	− 303	107 ± 31	2	969 ± 347	− 0.29 ± 0.10	19.9 ± 1.7
15/6 PM	− 5125	102 ± 14	17	906 ± 160	− 4.65 ± 0.82	15.2 ± 1.9
16/7	− 1234	67 ± 12	6	533 ± 133	− 0.66 ± 0.16	14.5 ± 1.9

pole-dipole survey, the current dipole is held fixed and the potential dipole (with the same electrode spacing as the current dipole) is circulated sequentially through all boreholes for all possible electrode pairs, after which the current dipole is moved (Figure 4a). For the horizontal dipole survey, it is important to choose a symmetric measurement sequence as described by Ramirez et al. (2003). The horizontal dipole-dipole survey employed for this study involves treating the borehole pairs A1-B1, A1-B2, A1-B4, A1-B5, B1-B2, B2-B4, B4-B5, and B5-B1 as sequential 2D panels (Figure 4b). For each 2D panel, the current dipole is held fixed and the potential dipole is circulated up and down the panel for all possible electrode pairs, after which the current dipole is moved.

Each acquisition sequence was designed to obtain full reciprocal data sets, with the current and potential dipoles interchanged to provide a measure of precision (LaBrecque et al., 1996). Including all reciprocals and before data filtering, the vertical dipole survey is comprised of 19,180 quadrupole measurements, and the horizontal dipole survey is comprised of 6048 quadrupole measurements.

ERT data analysis and inversion

The BHRS earth model is parameterized using a finite-volume mesh comprised of 241,472 conductivity cells ($56 \times 56 \times 77$) with 0.25-m cell sizes over the central borehole region. Outside of the borehole region, from ± 3.5 m outward and 17 m downward, the mesh is allowed to expand by a factor of 1.3 in all directions. The ERT data are normalized to a unit current (mV/mA) and inverted over the mesh using the 3D regularized least-squares Gauss-Newton inversion of Li and Oldenburg (2000). The regularization parameter is determined from a line search, and iteration proceeds until the misfit is equal to the level of noise assigned to the data. The data noise is assumed to be distributed normally with a standard deviation equal to a constant component of 2% of each datum, plus the reciprocal error (approximately equal to 2% of each datum), plus a constant floor of 0.08 V/A.

The objective function to be minimized is $\psi = \psi_d + \mu\psi_m$, where ψ is comprised of both a data component ψ_d and a model component ψ_m related by the regularization parameter μ. In the discrete case,

$$\psi = [\mathbf{W}_d(\mathbf{d} - f(\mathbf{m}))]^{\mathrm{T}}[\mathbf{W}_d(\mathbf{d} - f(\mathbf{m}))] + \mu[\mathbf{W}_m(\mathbf{m} - \mathbf{m}^{\mathrm{ref}})]^{\mathrm{T}}[\mathbf{W}_m(\mathbf{m} - \mathbf{m}^{\mathrm{ref}})], \quad (2)$$

where $\mathbf{d}$ is the vector of observed data (normalized potential differences), $\mathbf{m}$ is the vector of model parameters (log-transformed electrical conductivity), and f is the forward operator (the potential equation). The matrix $\mathbf{W}_d$ is the matrix of data weights, and the matrix $\mathbf{W}_m$ is the matrix of model weights comprised of both flatness and smallness components. The vector $\mathbf{m}^{\mathrm{ref}}$ is the reference model. Through $\mathbf{m}^{\mathrm{ref}}$, we incorporate prior or time-lapse information. For preinjection data, the reference model is a two-layer aquifer model based on water table measurements, fluid conductivity measurements, neutron porosity logs (Barrash and Clemo, 2002), and cross-borehole georadar estimates of porosity (Buursink, 2004). The aquifer model consists of an unsaturated zone to 1.9-m depth (σ = 0.2 mS/m) over a saturated zone (σ = 1.5 mS/m).

The estimated bulk electrical conductivity for the preinjection experimental stage σ_b^0 is shown in Figure 5. Geologic interpretation suggests a basic three-layer electrical earth model with a resistive unsaturated zone to 2-m depth (0.3 mS/m), a high-conductivity (high-porosity) zone from 2–3-m depth (5 mS/m), and a low-conductivity (low-porosity) zone to 16-m depth (1 mS/m), at which point the preinjection data lose reliability. Within the low-conductivity zone, two conductive features (~3 mS/m) are apparent at 5.5- and 12-m depth. These conductive features are interpreted as potential preferential flow paths that show up as high-porosity peaks in the neutron logs (Barrash and Clemo, 2002). In particular, the high-conductivity zone at 2–3-m depth corresponds well with a high-porosity

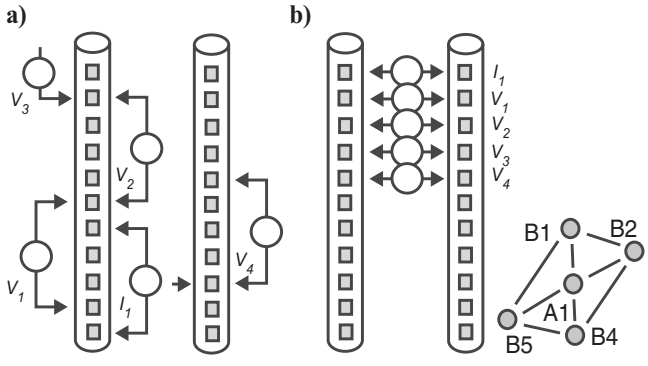

Figure 4. Schematic representation of survey geometries. I_1 indicates the first current dipole and V_i indicates the ith potential dipole for that current dipole. (a) Circulating skip-3 vertical dipole-dipole: multiple passes are made with the potential dipole through all boreholes in order to address every possible electrode pair with the given skip separation. (b) Horizontal dipole-dipole: data are collected in an arrangement of two-borehole panels as shown to the right.

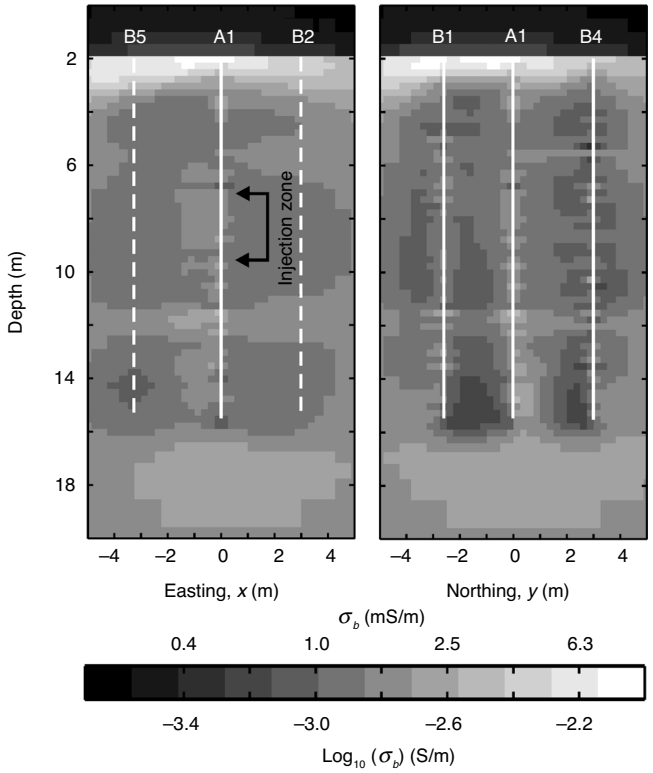

Figure 5. Estimated bulk conductivity for the background preinjection experimental stage. Vertical dipole data. Dashed vertical lines indicate out-of-plane boreholes; solid vertical lines indicate in-plane boreholes.

channel sand observed in both neutron log data and radar reflection data (Oldenborger et al., 2004). The vertically oriented artifacts are a result of our inability to fully recover the conductivity structure of the open boreholes resulting from discretization error and smoothing.

TIME-LAPSE ERT RESULTS

Every data set for each experimental stage was collected independently of the others and is assumed to represent a constant state of the aquifer over the collection interval. As such, each data set can be inverted independently and changes are isolated by postinversion model differencing. To test the benefit of incorporating information about past experimental stages, we perform the inversions using the three protocols: (1) independent regularization whereby the reference model for all inversions, at all experimental stages, is the constant two-layer aquifer model; (2) background regularization whereby the reference model for the preinjection inversion is the two-layer aquifer model, and the reference model for all subsequent experimental stages is the model obtained via inversion of the preinjection data; and (3) time-lapse regularization whereby the reference model for the preinjection inversion is the two-layer aquifer model, and the reference model for all subsequent experimental stages is the model obtained via inversion of the data from the previous stage. All other inversion parameters are held constant.

Figures 6 and 7 illustrate the inversion results using the independent protocol for both the vertical and horizontal dipole data, where the change in bulk conductivity from background $\Delta\sigma_b$ is isolated by subtracting the preinjection conductivity σ_b^0 (Figure 5). The tracer

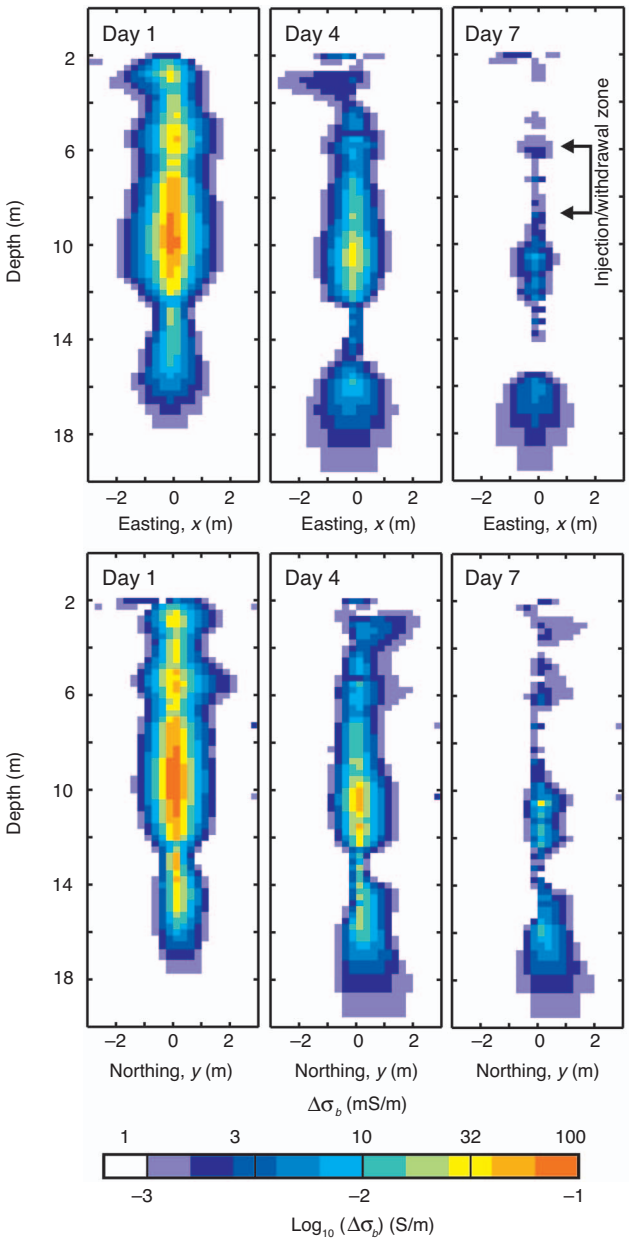

Figure 6. Change in estimated bulk conductivity from background for days 1, 4, and 7. Vertical dipole data.

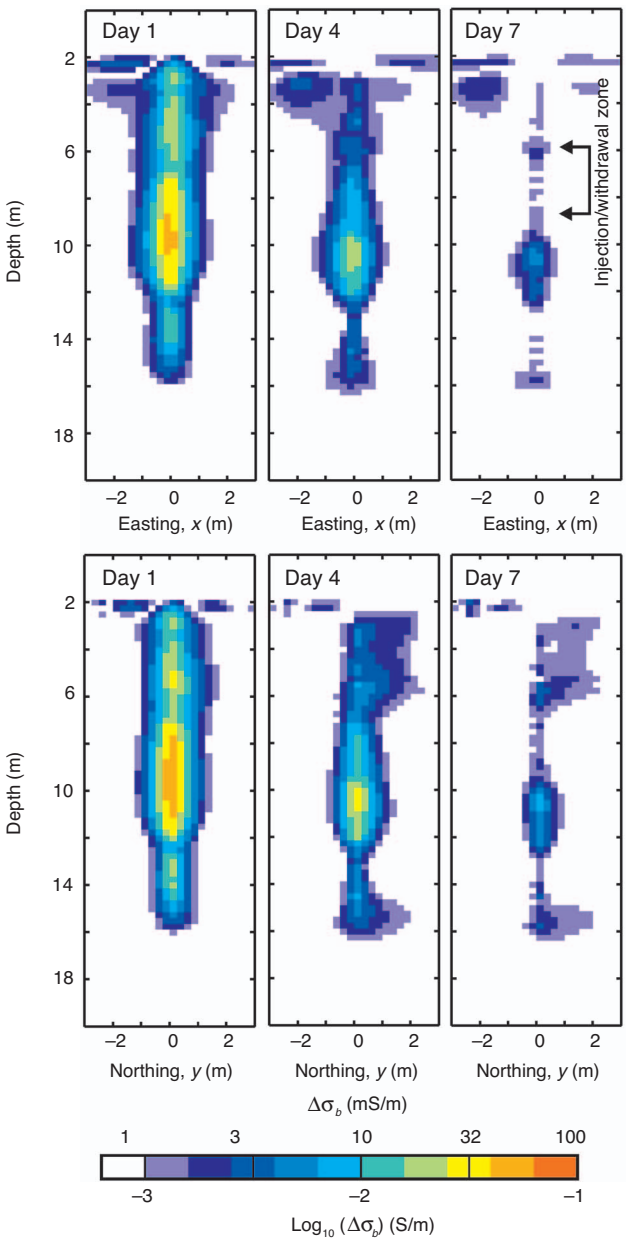

Figure 7. Change in estimated bulk conductivity from background for days 1, 4, and 7. Horizontal dipole data.

distribution is clearly evident in the differenced ERT images as an elevated conductivity. Both the vertical and horizontal dipole data result in estimated models that are in agreement with the qualitative water conductivity profiles (Figure 3). Solute is present over the entire sampled region, and the conductivity is observed to decrease over time in response to pumping. The maximum plume extent occurs outside of (below) the injection zone, which corroborates the hypothesis of short-circuiting of the packer system. Identification of preferential flow paths in the background ERT models is corroborated by the imaged shape of the tracer migration, particularly by the tracer fingering observed near 5.5-m depth. Despite withdrawal of several times the injected volume, the ERT results indicate that a significant amount of tracer remains in the aquifer by day 7. In particular, the high-conductivity changes at depth (Figures 6 and 7, days 4 and 7) are likely a result of density-dependent settling and represent solute that is irrecoverable via packed-zone pumping.

To compare regularization protocols, we examine the model objective function ψ_m, the regularization parameter μ, and the sum-squared model size $||\sigma_b||^2$ for both the vertical and horizontal survey geometries (Figures 8 and 9). According to equation 2, ψ_m is a measure of deviation from the reference. Time-lapse regularization consistently produces the smallest ψ_m because we are constantly updating the reference (Figures 8a and 9a). The value of ψ_m is variable for time-lapse regularization because the degree of change between experimental stages is variable. In fact, the variability in ψ_m can be interpreted as a measure of the relative change between the models at different experimental stages. Because ψ_m is small and variable, a large and variable trade-off parameter is required to stabilize the time-lapse inversions (Figures 8b and 9b). By the same arguments, ψ_m is relatively large and constant for the independent inversions (Figures 8a and 9a), and μ is relatively small and constant (Figures 8c and 9c). As the aquifer returns (via withdrawal) to the background state, ψ_m decreases slightly and μ increases slightly for the independent inversions. The values of ψ_m and μ are intermediate for the background inversions.

An interesting result is that time-lapse regularization consistently produces larger models (Figures 8c and 9c), although the trend is less pronounced for the vertical dipole data. We might think that inversions referenced to, and initiated by, previous models would require only small model modifications to satisfy the data. However, with time-lapse regularization, our objective function penalizes large perturbations from previous models as opposed to large perturbations from background. Thus, we are ultimately able to build up more structure in our final models, while still satisfying the data to the same level. Furthermore, fitting the data with time-lapse regularization requires less than half the number of nonlinear Gauss-Newton iterations required for the other inversion schemes.

As an example of the recovered models, Figure 10 illustrates the change in bulk conductivity from background at day 7 for the horizontal dipole data using each of the regularization protocols. It is clear that the regularization protocol has a significant impact on the estimated conductivity distribution. The conclusions drawn from these inversions will differ significantly in that the background-regularized inversion might suggest a fairly successful pump-and-cap-

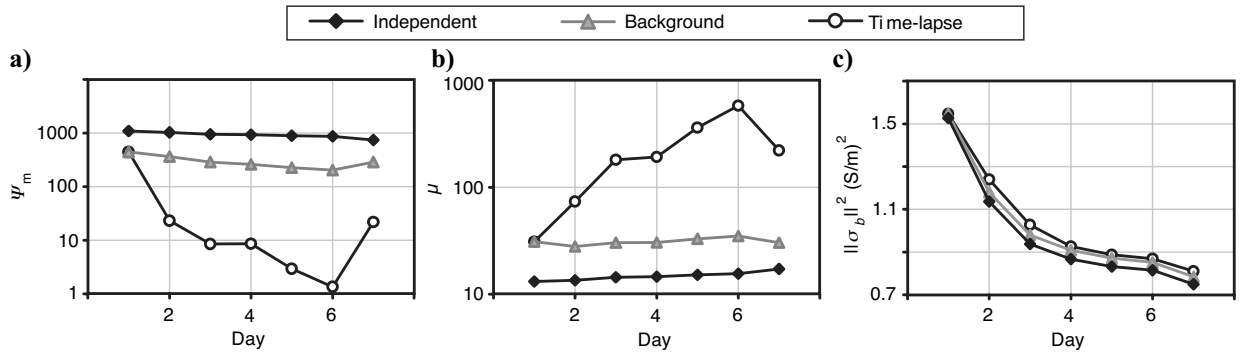

Figure 8. (a) Model objective function, (b) regularization parameter, and (c) sum-squared model size as a function of experimental stage for each of the inversion protocols. Vertical dipole data.

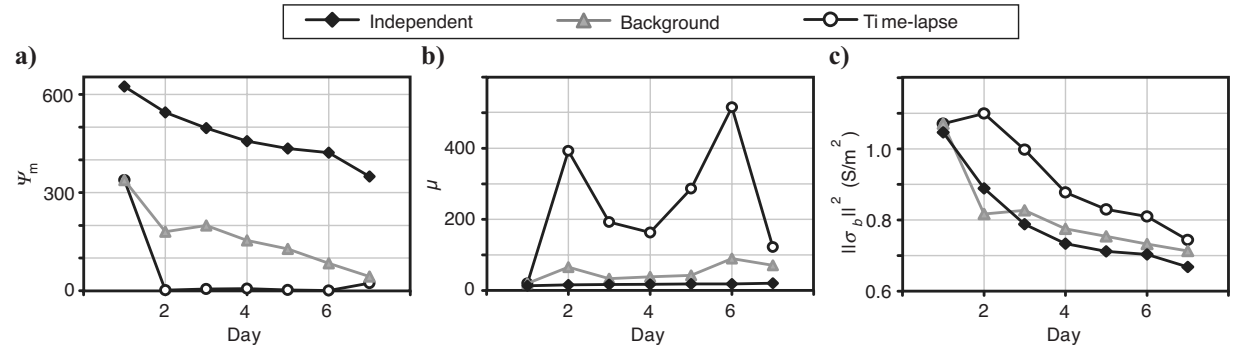

Figure 9. (a) Model objective function, (b) regularization parameter, and (c) sum-squared model size as a function of experimental stage for each of the inversion protocols. Horizontal dipole data.

ture effort with most of the solute being removed. Conversely, the time-lapse-regularized inversion suggests that a significant amount of solute remains in the aquifer, which is more consistent with water sample measurements (Table 1) and the phenomena of tailing or incomplete recovery in pump-and-treat applications (Domenico and Schwartz, 1998).

PREDICTING SOLUTE MASS

By integrating ERT-derived images of solute distribution, we can estimate solute mass within the aquifer as the zero-order moment of the concentration distribution. We use the concentration calibration equation 1 to convert fluid conductivity to solute concentration. To convert the ERT measure of bulk conductivity to fluid conductivity, we use Archie's Law as demonstrated by Kemna et al. (2002), Slater et al. (2002), Singha and Gorelick (2005), and Vanderborght et al. (2005). Archie's Law (Archie, 1942) is given by the empirical equation

$$\sigma_f = F\sigma_b, \tag{3}$$

which relates the bulk conductivity to the fluid conductivity by the formation factor F.

For long-term monitoring efforts, the temporal variability of environmental conditions may be important (Rein et al., 2004). At the timescale considered here, we assume F to be independent of time or conductivity, such that simple differencing yields

$$\Delta\sigma_f = F\Delta\sigma_b, \tag{4}$$

where $\Delta\sigma_f = \sigma_f - \sigma_f^0$ and $\Delta\sigma_b = \sigma_b - \sigma_b^0$. Figures 6 and 7 show that model differencing effectively accounts for a large portion of the persistent model error, such as borehole artifacts. Incorporating the concentration calibration equation 1, we have

$$C = X_{17}F\Delta\sigma_b. \tag{5}$$

A typical procedure is to assume a spatially invariant formation factor and to determine its approximate value through cross-plotting collocated measurements of fluid conductivity and bulk conductivity (e.g., Kemna et al., 2002; Singha and Gorelick, 2005). Alternatively, and in the absence of reliable data for variable fluid conductivity, we can use the measured background fluid conductivity and the background ERT estimate of bulk conductivity to calculate a spatially variable formation factor $F(\mathbf{r}) = \sigma_f^0/\sigma_b^0(\mathbf{r})$ (e.g., Slater et al., 2002). However, in using this technique, any nonearth variability in the preinjection conductivity model (Figure 5) will contaminate the formation factor through σ_b^0. To avoid this pitfall, we limit ourselves to the 1D bulk conductivity at the boreholes to obtain $F(z) = \sigma_f^0/\sigma_b^0(z)$ and a vertically averaged $F^* = 13 \pm 4$, where the error is reported as one standard deviation of the spatial variability.

As a comparison, we also calculate the formation factor based on independent 1D porosity information. We adopt the porosity-based formation factor $F = n^{-m}$, where n is the porosity and m is the shape factor (Jackson et al., 1978). Using the bulk conductivity from preinjection ERT models in the near-borehole region and the constant background fluid conductivity, we predict the porosity for any given m according to

$$n(z) = [\sigma_b^0(z)/\sigma_f^0]^{(1/m)}. \tag{6}$$

By minimizing the sum-squared difference between the ERT-estimated porosity and the neutron-log porosity (Barrash and Clemo, 2002), we estimate the best-fit shape factor of $m = 1.7$. This shape factor is consistent with estimates for m at a nearby unconsolidated aquifer (Barrash et al., 1997). Given m, the vertically variable $F(z) = n(z)^{-m}$ is calculated using the neutron porosity and we again obtain $F^* = 13 \pm 4$.

For simplicity, and to avoid unwarranted propagation of 1D variability (or lack thereof) to 3D, we utilize the vertically averaged formation factor F^* for the mass-estimation procedure. By the same argument, we utilize the vertically averaged porosity $n^* = 0.22 \pm 0.03$ for the central region of the BHRS. Solute mass is then calculated over the finite-volume mesh as a summation

$$M = n^* \sum_i V_i C_i, \tag{7}$$

where V_i and C_i are the volume and concentration of the ith cell in the discretized earth model.

Total solute mass

Time series for solute mass predictions are shown in Figure 11 for both data types. Error bars on the solute mass as predicted by water samples (Table 1) represent the propagation of the experimental errors on X and σ_f (equation 1). Error bars on ERT-predicted mass represent the propagation of the spatial variability of n and F and the experimental error on X (equations 7 and 5, respectively). Although the ERT-predicted mass compares to the water sample mass within the relative error bounds for the vertical dipole data, solute mass is underpredicted consistently using ERT for both data types and all regularization protocols. For the vertical dipole data (Figure 11a), the es-

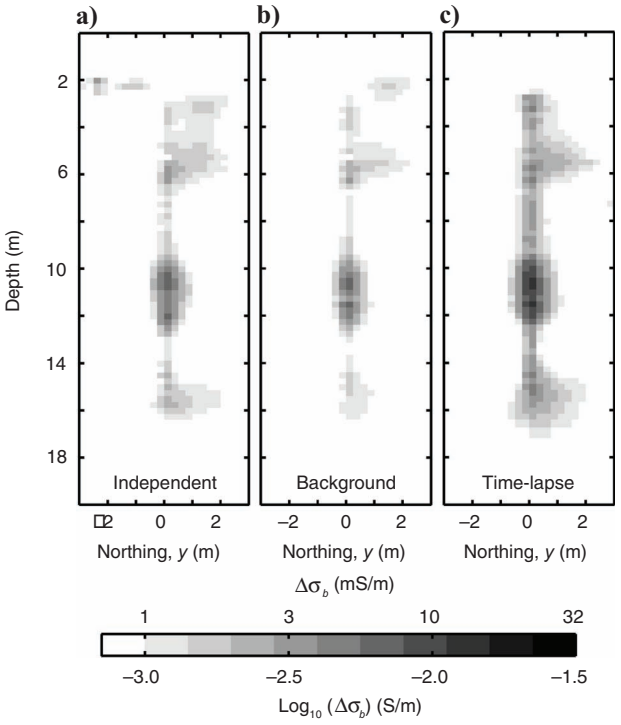

Figure 10. Change in estimated bulk conductivity from background for day 7 using (a) independent regularization, (b) background regularization, and (c) time-lapse regularization. Horizontal dipole data.

timated mass is somewhat sensitive to the regularization protocol. The independent inversions result in slightly larger mass than the time-lapse inversions. Although time-lapse inversions produce the largest models independently (Figures 8c and 9c), solute mass is a function of the model change from background. For the horizontal dipole data (Figure 11b), the difference in regularization schemes is more pronounced, with the largest (most accurate) mass predicted using the time-lapse inversion protocol. In both cases, background regularization results in the least model change and the lowest estimated mass.

Figure 12 illustrates the accuracy of ERT mass prediction. Similar to the observations for model size, the vertical dipole data exhibit significantly larger mass estimates than the horizontal dipole data. At best, our ERT estimates represent approximately 85% (vertical dipoles, Figure 12a) and 60% (horizontal dipoles, Figure 12b) of the total solute mass in the aquifer. It is well recognized that smoothness-constrained, least-squares inversion underpredicts magnitude and overpredicts extent of conductivity variations (e.g., Ramirez et al., 2003). However, the two phenomena do not balance under integration, and the result is a mass deficit whereby the overextent does not account for the reduced magnitude. The discrepancy between data sets is likely a result of the larger volume of investigation for the vertical dipole data and the subsequent ability to better image the sinking solute. As we have quantified it, the errors associated with assuming a spatially invariant petrophysical transform (error bars in Figures 11 and 12) are insufficient to explain the observed mass deficit for the horizontal dipole data and are unconvincing at explaining the systematic underprediction of mass. However, the observed variability of the formation factor and the porosity are significant and may be exacerbated by the spatially integrated nature of mass estimates. That is, where F is low, n is high, and C may be high in areas of predominantly high or low n. How this spatially dependent interaction will affect mass estimates is not predicted easily without modeling the spatial variability of the petrophysical properties themselves.

For a similar experiment, Binley et al. (2002) observe a 50% mass deficit, which they attribute to a loss of resolution over portions of the inter-borehole model domain, and Ramirez et al. (2003) note a similar dependence of the model magnitude on resolution. In our case, spatially variable resolution might require a spatially variable calibration involving an increase in an effective formation factor away from the boreholes to account for underprediction of conductivity by the smooth least-squares inversion. This correlation loss described by Day-Lewis et al. (2005), whereby geophysical-hydrogeologic calibrations performed in the lab or at a borehole may not apply over an entire tomographic image, will contribute further to our underestimation of solute mass.

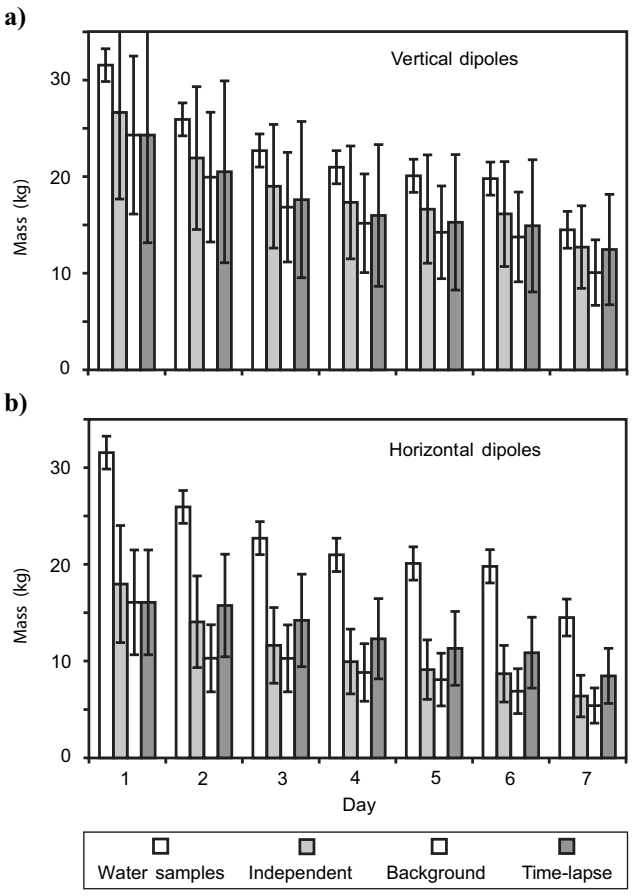

Figure 11. Time series of total solute mass in the aquifer obtained from water sample measurements and as predicted by ERT using the three inversion protocols. (a) Vertical and (b) horizontal dipole data.

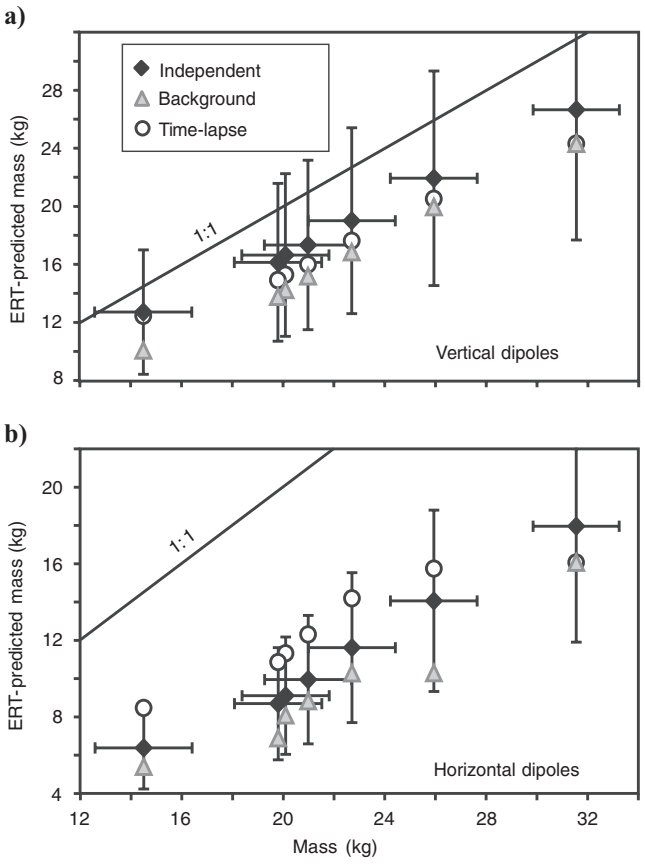

Figure 12. Comparison of total solute mass in the aquifer obtained from water sample measurements with that predicted by ERT for the three inversion protocols. (a) Vertical and (b) horizontal dipole data (note the different scale). Error bars are illustrated for the independent inversion protocol only.

Withdrawn solute mass

This experimental study is unique in that, rather than monitoring solute migration as in the aforementioned tracer studies, we are able to examine changes in solute mass in the aquifer through the process of sequential solute withdrawal. Given mass equation 7, for any two experimental stages, the withdrawn mass is estimated by

$$M_W = M^2 - M^1 = n^* F^* X_{17} \sum [V(\Delta\sigma_b^2 - \Delta\sigma_b^1)], \quad (8)$$

where the i subscript has been dropped. By expanding the conductivity terms to $\Delta\sigma_b = \sigma_b - \sigma_b^0$, we cancel out subtraction of the background model such that

$$M_W = n^* F^* X_{17} \sum [V(\sigma_b^2 - \sigma_b^1)]. \quad (9)$$

For withdrawn mass, we are dealing only with the instantaneous model change, as opposed to the change from background.

Figure 13 illustrates the time series of ERT-predicted mass withdrawn from the aquifer. On days 2 and 7, the withdrawn mass is large and the prediction accuracy is poor (on day 3 as well for the horizontal dipole data). However, on intermediate days, the ERT predictions are reliable and do not exhibit consistent under- or overprediction. Figure 14 illustrates the comparison of ERT-predicted mass to the mass obtained from water sample measurements (Table 1). ERT is better at predicting the withdrawn mass (the change in mass between experimental stages) as opposed to the total solute mass in the aquifer. Furthermore, prediction accuracy is independent of the regularization protocol, allowing us to take advantage of the computational savings of time-lapse regularization. The increased prediction accuracy for withdrawn mass implies that we can estimate the rate of change of solute mass well, but not the total quantity. Such an approach does not require background data, and can therefore be applied at previously contaminated sites.

However, Figure 14 also demonstrates that, as the change in mass between experimental stages increases, the accuracy of ERT predictions of withdrawn mass breaks down. Calculation of M_W still involves model differencing and, as the withdrawn solute mass increases, the magnitude of the model change increases, and our ability to predict M_W degrades. Because the estimate of M_W is less accurate as M_W increases, we posit that ERT postinversion model differencing is stable, provided that model changes are not too large. When model changes become too large, model dependence of the inversion is manifest as unstable differencing that precludes accurate prediction of mass or withdrawn mass. In this case, too large is approximately 3–4 kg of solute mass for the vertical dipole data and approximately 2 kg of solute mass for the horizontal dipole data. The implication for general monitoring efforts is that data should be collected as frequently as possible to allow for accurate model differencing.

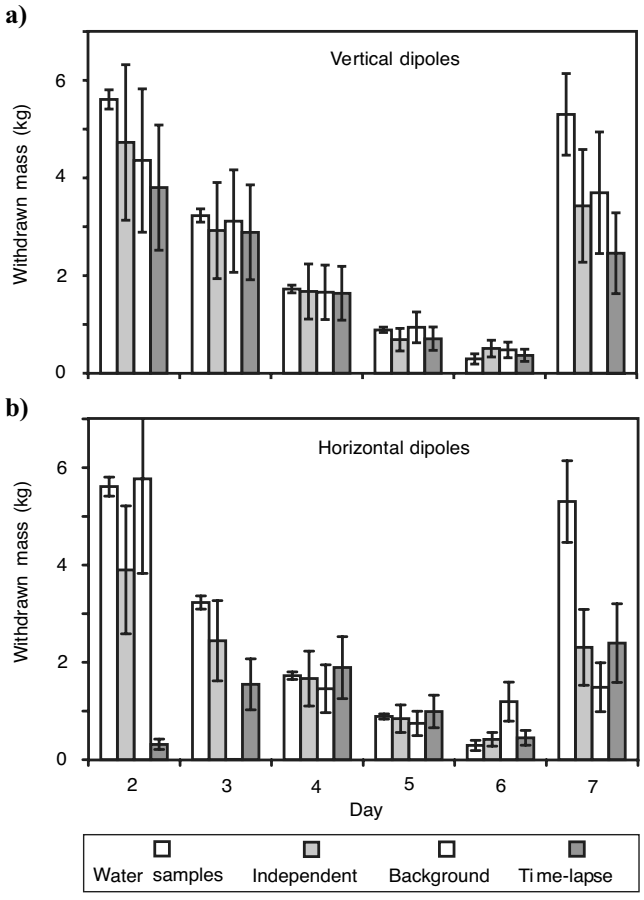

Figure 13. Time series of withdrawn solute mass obtained from water samples and as predicted by ERT using the three inversion protocols. (a) Vertical and (b) horizontal dipole data.

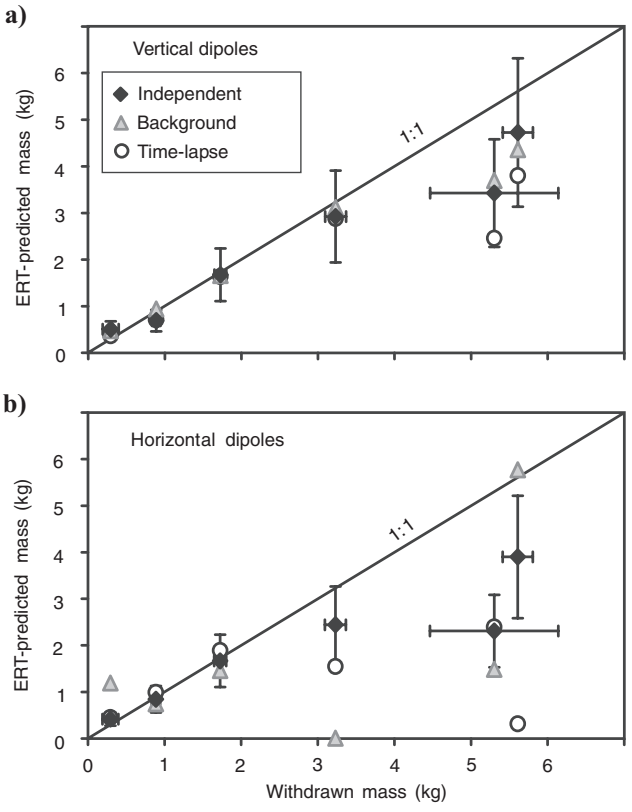

Figure 14. Comparison of withdrawn solute mass obtained from water sample measurements with that predicted by ERT for the three different inversion protocols. (a) Vertical and (b) horizontal dipole data. Error bars are illustrated for the independent inversion protocol only.

CONCLUSIONS

A conductive KBr solution was injected and sequentially withdrawn from a near-surface alluvial aquifer as a proxy for monitoring a pump-and-capture remediation effort using ERT. Postinjection ERT images of bulk conductivity clearly illustrate the emplacement of the KBr solution and its sequential withdrawal in response to pumping. Time-lapse ERT images are consistent with multilevel water samples and demonstrate tailing of the pump-and-capture effort. Significant solute mass is imaged in the aquifer after pumping of several times the contaminant volume.

The sequential withdrawal of KBr solution and collection of data over time allowed for testing of three different regularization protocols for incorporating time-lapse information. Time-lapse regularization (whereby the inverted model from the previous experimental stage is used as a reference) results in the largest models and requires far fewer iterations for the inversion algorithm to converge. For large 3D problems, this speedy convergence leads to significant computational savings.

Changes in the bulk conductivity from the preinjection experimental stage were used to estimate solute mass in the aquifer as a function of time. When estimating solute mass, the borehole and other artifacts are effectively removed via background subtraction. However, these artifacts prevent calculation of spatially variable porosity or formation factor from the background conductivity models. Instead, we utilize independent neutron porosity logs to calibrate Archie's Law for estimating solute mass. We find that, at any experimental stage, we are able to estimate total solute mass in the aquifer with a maximum accuracy of 85% and 60% for the vertical and horizontal dipole-dipole data, respectively. Accuracy of mass prediction is also dependent on the regularization protocol with the largest variation observed for the horizontal dipole data. Error associated with our inability to represent the 3D spatial variability of the petrophysical parameters is sufficient to account for the mass deficit in some, but not all cases. Moreover, consistent underestimation of solute mass is not adequately explained by spatial variability of the petrophysical parameters. However, because we have employed a 1D calibration of Archie's Law, we may observe correlation loss, whereby the calibration developed at the borehole is not representative over the entire aquifer because of variable resolution of the inversion procedure. Additional errors in calibration and parameter conversion may arise as a result of temperature fluctuations and temporal variability of other variables, a factor of significant concern for long-term monitoring efforts.

The consistent underestimation of solute mass suggests the ability to accurately estimate rates of change. In addition to total solute mass, we estimate the withdrawn solute mass for every experimental stage. We find that estimates of withdrawn mass are accurate for changes in mass below 3–4 kg for vertical dipole data and below 2 kg for horizontal dipole data, regardless of regularization protocol. Estimating the withdrawn solute mass does not require background subtraction and, thus, does not require background data. As the withdrawn solute mass increases, the magnitude of the model change increases and differencing of contiguous models becomes unstable, such that we cannot accurately predict either the total mass or the withdrawn mass. For this experiment, horizontal dipole data sets are less robust in their ability to represent model change in terms of total solute mass or withdrawn mass. The discrepancy between the vertical and horizontal dipole data with respect to mass prediction accuracy and regularization dependence is suspected to be a manifestation of the larger and more reliable volume of investigation for the vertical dipole data.

ACKNOWLEDGMENTS

This research was funded by the Natural Sciences and Engineering Research Council of Canada, the Inland Northwest Research Alliance, EPA grant X970085-01-0, and NSF-EPSCOR grant EPS0132626. W. Barrash, R. Sharpe, T. Johnson, and M. Buursink were instrumental in experimental design and execution. Two anonymous reviewers provided comments and criticisms that resulted in an improved manuscript. The University of British Columbia Geophysical Inversion Facility provided DCIP3D, a program library for forward modelling and inversion of DC resistivity and induced polarization data over 3D structures, developed under the consortium research project: Inversion of 3D Resistivity and Induced Polarization Data.

REFERENCES

Archie, G. E., 1942, The electrical resistivity log as an aid in determining some reservoir characteristics: Transactions of the American Institute of Mining, Metallurgical, and Petroleum Engineers, **146**, 54–62.

Barrash, W., and T. Clemo, 2002, Hierarchical geostatistics and multifacies systems: Boise Hydrogeophysical Research Site, Boise, Idaho: Water Resources Research, **38**; http://dx.doi.org/10.1029/2001WR001259.

Barrash, W., R. Morin, and D. M. Gallegos, 1997, Lithologic, hydrologic and petrophysical characterization of a coarse-grained, unconsolidated aquifer, Capital Station site, Boise, Idaho: Symposium on Engineering Geology and Geotechnical Engineering, Proceedings, 307–323.

Barrash, W., and E. C. Reboulet, 2004, Significance of porosity for stratigraphy and textural composition in subsurface, coarse fluvial deposits: Boise Hydrogeophysical Research Site: Geological Society of America Bulletin, **116**, 1059–1073.

Bentley, L. R., and M. Gharibi, 2004, Two- and three-dimensional electrical resistivity imaging at a heterogeneous remediation site: Geophysics, **69**, 674–680.

Binley, A., G. Cassiani, R. Middleton, and P. Winship, 2002, Vadose zone model parameterisation using cross-borehole radar and resistivity imaging: Journal of Hydrology, **267**, 147–159.

Buursink, M. L., 2004, First-order characterization of electromagnetic propagation velocity at the Boise Hydrogeophysical Research Site using borehole radar methods: 74th Annual International Meeting, SEG, Expanded Abstracts, 1464–1467.

Daily, W., A. Ramirez, A. Binley, and D. LaBrecque, 2004, Electrical resistance tomography: The Leading Edge, **23**, 438–442.

Day-Lewis, F. D., J. M. Harris, and S. W. Gorelick, 2002, Time-lapse inversion of crosswell radar data: Geophysics, **67**, 1740–1752.

Day-Lewis, F. D., K. Singha, and A. M. Binley, 2005, Applying petrophysical models to radar travel time and electrical resistivity tomograms: Resolution-dependent limitations: Journal of Geophysical Research, **110**, B08206; http://dx.doi.org/10.1029/2004JB003569.

Domenico, P. A., and F. W. Schwartz, 1998, Physical and chemical hydrogeology, 2nd ed.: John Wiley & Sons.

Hanke, M., and C. W. Groetsch, 1998, Nonstationary iterated Tikhonov regularization: Journal of Optimization Theory and Applications, **98**, 37–53.

Hausrath, E., W. Barrash, and E. Reboulet, 2002, Water sampling and analysis for the tracer/time-lapse radar imaging test at the Boise Hydrogeophysical Research Site: Technical report CGISS 02-03, Boise State University.

Hyndman, D. W., and S. M. Gorelick, 1996, Estimating lithologic and transport properties in three dimensions using seismic and tracer data: The Kesterson aquifer: Water Resources Research, **32**, 2659–2670.

Jackson, P. D., D. T. Smith, and P. N. Stanford, 1978, Resistivity-porosity-particle shape relationship for marine sands: Geophysics, **43**, 1250–1268.

Kemna, A., J. Vanderborght, B. Kulessa, and H. Vereecken, 2002, Imaging and characterisation of subsurface solute transport using electrical resistivity tomography (ERT) and equivalent transport models: Journal of Hydrology, **267**, 125–146.

LaBrecque, D. J., M. Miletto, W. Daily, A. Ramirez, and E. Owen, 1996, The effects of noise on Occam's inversion of resistivity tomography data: Geophysics, **61**, 538–548.

LaBrecque, D. J., and X. Yang, 2001, Difference inversion of ERT data: A fast inversion method for 3-D in situ monitoring: Journal of Environmen-

tal and Engineering Geophysics, **6**, 83–89.
Li, Y., and D. W. Oldenburg, 2000, 3-D inversion of induced polarization data: Geophysics, **65**, 1931–1945.
Loke, M. H., 1999, Time-lapse resistivity imaging inversion: Environmental and Engineering Geophysical Society European Section, Meeting, Proceedings, Em1.
Oldenborger, G. A., M. D. Knoll, and W. Barrash, 2004, Effects of signal processing and antenna frequency on the geostatistical structure of ground-penetrating radar data: Journal of Environmental and Engineering Geophysics, **9**, 201–212.
Ramirez, A. L., R. L. Newmark, and W. D. Daily, 2003, Monitoring carbon dioxide floods using electrical resistance tomography (ERT): Sensitivity studies: Journal of Environmental and Engineering Geophysics, **8**, 187–208.
Ramirez, A. L., J. J. Nitao, W. G. Hanley, R. Aines, R. E. Glaser, S. K. Sengupta, K. M. Dyer, T. L. Hickling, and W. D. Daily, 2005, Stochastic inversion of electrical resistivity changes using a Markov Chain Monte Carlo approach: Journal of Geophysical Research, **110**, B02101; http://dx.doi.org/10.1029/2004JB003449.
Rein, A., R. Hoffmann, and P. Dietrich, 2004, Influence of natural time-dependent variations of electrical conductivity on DC resistivity measurements: Journal of Hydrology, **285**, 215–232.
Singha, K., and S. M. Gorelick, 2005, Saline tracer visualized with three-dimensional electrical resistivity tomography: Field-scale spatial moment analysis: Water Resources Research, **42**, W05023; http://dx.doi.org/10.1029/2004WR003460.
Slater, L., A. Binley, R. Versteeg, G. Cassiani, R. Birken, and S. Sandberg, 2002, A 3D ERT study of solute transport in a large experimental tank: Journal of Applied Geophysics, **49**, 211–229.
Slater, L. D., and S. K. Sandberg, 2000, Resistivity and induced polarization monitoring of salt transport under natural hydraulic gradients: Geophysics, **65**, 408–420.
Vanderborght, J., A. Kemna, H. Hardelauf, and H. Vereecken, 2005, Potential of electrical resistivity tomography to infer aquifer transport characteristics from tracer studies: A synthetic case study: Water Resources Research, **41**, W06013; http://dx.doi.org/10.1029/2004WR003774.
Zhou, B., and S. A. Greenhalgh, 2000, Cross-hole resistivity tomography using different electrode configurations: Geophysical Prospecting, **48**, 887–912.